INDIAN JOURNAL OF SCIENCE AND TECHNOLOGY

RESEARCH ARTICLE

∗**Corresponding author**.
P V Lakshmi Narayana

Department of Nuclear Physics, Andhra University, Visakhapatnam, 530003, A.P, India
pvl.nuclearphysics@gmail.com

Competing Interests: None

Synthesis and characterization of Fe$_2$O$_3$-Bi$_2$O$_3$-TiO$_2$ nanoparticles and its magnetic properties

Tentu Manohra Naidu[1], P V Lakshmi Narayana[1]∗

1 Department of Nuclear Physics, Andhra University, Visakhapatnam, 530003, A.P, India

Abstract

Objectives: The current research work was investigated magnetic properties of Fe$_2$O$_3$-Bi$_2$O$_3$-TiO$_2$ nanoparticles (NP$_S$). **Methods/Statistical analysis**: The Fe$_2$O$_3$-Bi$_2$O$_3$-TiO$_2$ has been synthesized by a simple precipitation method. The samples were characterized by X-ray powder diffraction (XRD), field emission scanning electron microscopy (FESEM), transmission electron microscopy (TEM), Fourier-Transform Infrared Spectroscopy (FTIR) and UV-vis. absorption (reflectance) spectra. The magnetic properties of the magnetite nanoparticles were calculated by vibrating sample magnetometer (VSM) at ambient temperature. **Findings:** The effect of calcination on the magnetic and structural properties of Fe$_2$O$_3$-Bi$_2$O$_3$-TiO$_2$ nanoparticles was studied. The Fe$_2$O$_3$-Bi$_2$O$_3$-TiO$_2$ nanocrystal was subjected to calcination up to 200°C, magnetite was converted to magnetite; the second transition was in the range of 300-400°C which changed it to hard ferromagnetic hematite. **Application/Improvements:** This research provides promising results concerned with magnetic sensing probes for magnetic resonance imaging for in-vitro diagnostics and contrast agents.

Keywords: Fe2O3-Bi2O3-TiO2 NPs; Magnetic Properties; XRD; FESEM; VSM

1 Introduction

The use of nanomaterials for water purification has become an interesting research area in recent years. Nanomaterials are a growingly important nanotechnology products. They contain nanoparticles in at least one dimension which are smaller than 100 nm. These nanomaterials are coming into health care, electronics, cosmetics and other areas[1,2]. Due to many potential innovative applications, Nanoparticles research has received considerable attention. They have unique and novel magnetic, optical, electronic and catalytic properties[3].

Magnetite is known as the black iron oxide and the oldest known source of magnetic oxides. Especially hematite and maghemite, have been used as pigments since ancient times to give pottery reddish coloration. Similar to hematite, magnetite is a semiconductor with a band gap of around 2 eV, although the specific value of the gap based on the electron spin[4,5]. The iron atom has a strong magnetic moment in its 3D orbitals, due to four unpaired electrons. Paramagnetic materials reveal randomly

distributed dipoles in the absence of the magnetic field. The magnetic response of the paramagnetic materials is relatively weak. Ferromagnetic materials are characterized by their spontaneous magnetization regardless of the absence or presence of an external magnetic field. The magnetic moments are aligned parallel in one specific direction depending on the crystal structure. The ferromagnetism originates from exchange interactions occurring in ordered magnetic solids. The difference between ferromagnetic and ferrimagnetic materials is related to the alignment of adjacent dipoles. In ferrimagnetic materials, nonmagnetic field weaker magnetic dipoles aligned antiparallel to their adjacent stronger dipoles reduces the net magnetization. The most common iron oxide (Fe_2O_3) has important magnetic properties as well. From the standpoint of basic research, iron (III) oxide is a convenient compound for the general polymorphism study and nanoparticles ' magnetic and structural phase transitions. It is well established that amorphous Fe_2O_3 and four polymorphs (alpha, beta, gamma, and epsilon) exist[6]. The most common polymorphic structure "alpha" (hematite) with hexagonal rhombohedral, prototype corundum structures, and "gamma" (maghemite) cubic spinel structure was found in nature. At a temperature of 650° C, hematite turns into Fe_3O_4 with a high energy loss. The Bim + 1Fem – $3Ti_3O_3$m + 3 compounds combine ferroelectric, Semiconducting and ferromagnetic properties[7–9], making them potentially attractive to applications in electrical engineering, e.g. as magnetic recording media. The Electrical properties of compounds have been observed in the Bi_2O_3–TiO_2–Fe_2O_3 system[10–13]. Nature and conduction mechanism of a dielectric relaxation model proposed by Jonscher is interrelated[14]. Literature reports are available on the synthesis of TiO_2-based magnetic photocatalysts[15]. Several complexes such as Fe_2O_3, WO_3, $BiVO_4$, Bi_2WO_6, and Ag_3PO_4 have been tested as visible light photocatalyst[16]. Our investigation mainly focused on the synthesis of Fe_2O_3-Bi_2O_3-TiO_2 nanoparticles and the observation of magnetic properties of nanoparticles as a function of nanoparticle morphologies.

2 Experimental

2.1 Materials and methods

All analytical grade chemicals were used in the experiment. Double distilled water was used for all experiments. Co-doped nanoparticles were prepared by using the following protocol. Nano iron (**II**, **III**) oxide (Spherical, diameter 20nm, 99.5%) was purchased from Shanghai Chemical Co., Ltd., China. Ammonia solution and isopropyl alcohol were obtained from Merck Ltd. Bismuth Nitrate (Bi_2NO_3) and tetra butyl titanate (TBOT) were purchased from Merck, China. Anhydrous ethanol was obtained from Hangzhou Changzheng Chemical Reagent Co., Ltd., China.

2.2 Catalyst preparation

2.2.1 Preparation of Fe_3O_4-Bi_2O_3 nanoparticles
The Fe_3O_4 NPs (0.25 g) were sonicated for 1hr, allowing anhydrous ethanol (40 mL) to disperse uniformly. Concentrated ammonium hydroxide (4.5 mL) was diluted to the above solution, and 0.75 g of Bi $(NO_3)_3$ $5H_2O$ was quickly added under intense stirring. The solution was left up to heat for 12 hr. The commodity was obtained by centrifugation and washed with anhydrous ethanol three times.

2.2.2 Preparation of Fe_2O_3-Bi_2O^3-TiO_2 nanoparticles
Their sultan's product was redisposed in anhydrous ethanol (40mL). Subsequently, a proper amount of TBOT (5.0mL) dissolved in isopropyl alcohol (40.0mL) was introduced to the system drop wise, followed by heating the solution at about70°C. The entire process underwent vigorous stirring. The reddish-brown precipitate was washed with distilled water and ethanol five times after 12h and dried in a vacuum oven at 80° C for 24 hr. They eventually calcinated the items at 500° C for 2hr.

2.2.3 Characterization of magnetic nanoparticles
A Shimadzu UV-1700 spectrophotometer was used to test the UV — Vis absorption spectra. A Shimadzu X-ray diffractometer equipped with Cu Kα radiation source using Ni as a filter configuration of 45 kV/40 mA was used to analyze the crystalline existence of NPs. A total of 2 scans ranging from 10 to 90. KBr pellet method was used to obtain the Fourier transform infrared spectra (FT-IR) in the range 4,000 to 400 cm^{-1}. They collected the FE-SEM micrographs using a JEOL 6335F FE-SEM. The particle size and morphology of the sample were analyzed by transmission electron microscopy (TEM), and UV-vis absorption spectrum diffuse reflectance (UV-Vis DRS) was measured using a UV-vis spectrometer (U-4100, Hitachi).

2.2.4 Vibrating sample Magnetometer (VSM)
Using the Vibrating Sample Magnetometer (VSM) test, to determine the macroscopic magnetic properties of the nanoparticles Fe_2O_3-Bi_2O_3-TiO_2. The VSM was completed at room temperature. The vibrating sample magnetometer (VSM) is one of

the most successful implementations of a magnetometer. In comparison with alternating gradient magnetometer, the VSM is indifferent to the mass and size of the sample up to a considerable range. The sample is inserted in a constant uniform external magnetic field that induces a sample magnetization. It causes disturbances in the external magnetic field when the magnetized sample is then vibrated. A set of coils or some magnetic field sensors can be arranged around the sample to measure these perturbations. For example in the case of coils, magnetic flux piercing the coils will change resulting in the generation of an EMF (electromotive force) in coils. The VSM can measure the magnetic susceptibility, at room temperature, of magnetic nanostructured samples. For this scheme, the first crucial step in the construction of a vibrating mechanism that can vibrate the sample with measurable and controllable amplitude. Then we need an electromagnet to provide the magnetic field required to magnetize the sample. Finally, detection coils are required to detect the magnetic field perturbations produced by vibrating the magnetized sample in the applied magnetic field.

3 Results and Discussion

3.1 XRD patterns

The inset from Figure 1 is the extended crystal plane XRD peaks (101) for all the samples. The well-defined diffraction peaks are approximately 25, 38, 48, 54, 54, 54, 62, 68, 70, 70, 70, 74, and 82, which are assigned to the crystal planes (101), (004), (200), (105), (211), (204), (116), (220), (215) and (224) respectively. This characteristic pattern of the XRD is consistent with the typical anatase TiO_2 JCPDS values (JCPDS Card No. 21-1272). In the curves, the diffraction peaks of the crystal planes (101), (200) and (004) are used to determine the sample lattice parameter and crystal dimension. The cell volume of Fe_2O_3-Bi_2O_3-TiO_2 is much greater than that of un-doped TiO_2. The experimental constants ' a','b ' and ' c ' are determined from the XRD peak 101, 004 and 200 of the XRD sequence ' a'='b ' is 3.780 Å and ' c ' is 9.52 Å unit cell volume V=134.94 Å. The calculated average crystallite size, D is 60 ± 0.5 nm. Using Scherer's equation:

$$D = \frac{0.9\,\lambda}{\beta \cos \theta}$$

Where,

D is the average crystallite size,

λ the X-ray wavelength,

β the angular line width at half maximum intensity,

θ Bragg's angle.
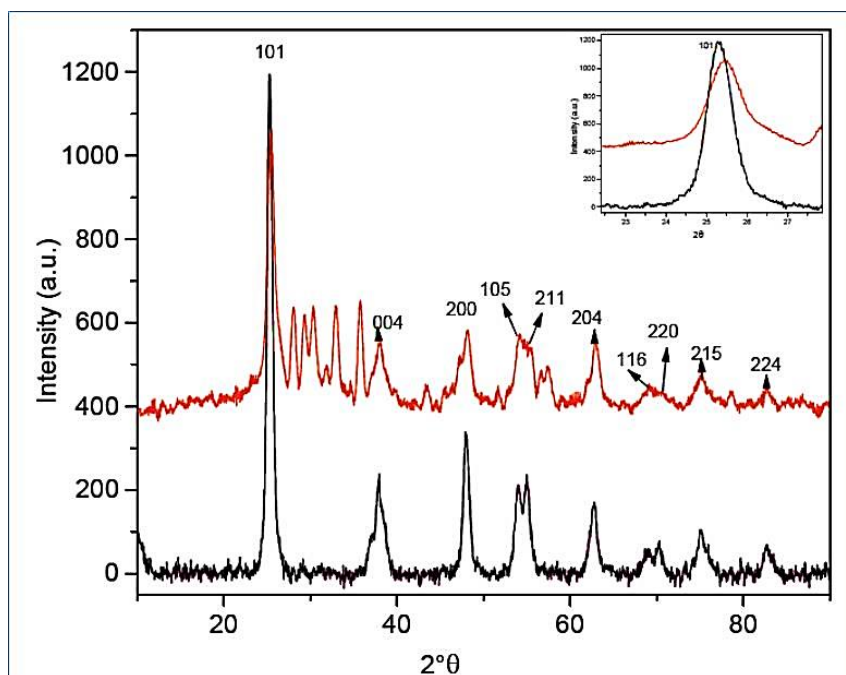
Fig 1. XRD patterns of un-doped TiO_2 and Fe_2O_3-Bi_2O_3-TiO_2. Inset is the enlarged XRD peaks of crystal plane (101)

3.1.1 *UV-Vis DRS*

Figure 2 shows the UV-Vis DRS absorption spectra of un-doped TiO_2, Fe_2O_3-Bi_2O_3, and Fe_2O_3-Bi_2O_3-TiO_2 samples. Un-doped TiO_2 and Fe_2O_3-Bi_2O_3-TiO_2 are strongly absorbed in the UV region due to the band-to-band transition. Compared to pure TiO_2, 1.00 percent of Fe-Bi_2O_3/TiO_2 presents a small hump at around 480 nm in the visible-light region.
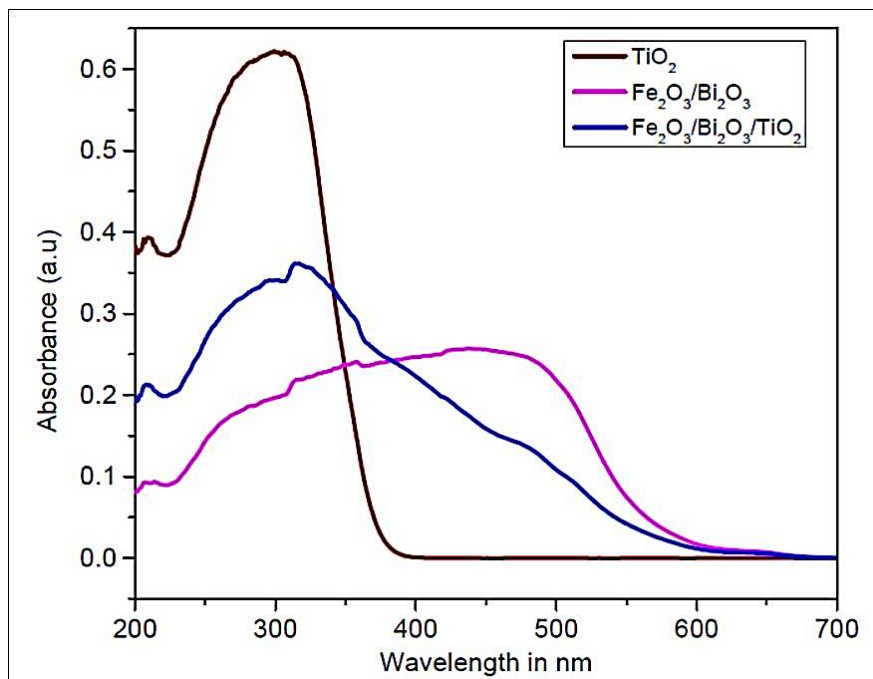

Fig 2. Gives UV-Vis DRS absorption spectra of (a) un-dopedTiO_2 (b) Fe_2O_3-Bi_2O_3, (c) Fe_2O_3-Bi_2O_3-TiO_2

3.1.2 *FT-IR*

FT-IR was used to characterize the composition and structure of the Fe_2O_3-Bi_2O_3 and Fe_2O_3-Bi_2O_3-TiO_2. As shown in Figure 3, the Fe_2O_3-Bi_2O_3-TiO_2. Composites possess more signals than Fe2O3. It has been reported that the signal at the wave number around 800 cm^{-1} corresponds to the symmetric vibration of Ti-O-Ti., 1080 cm^{-1} for asymmetric stretching vibration of Ti-O-Ti.TiO2 exists as amorphous phase was confirmed by combining the results of FT-IR and XRD. The presence of water is evidenced by the appearance of the bending mode at 1630cm^{-1} and the stretch in mode at 3370cm^{-1}.

3.2 SEM analysis of Fe_2O_3-Bi_2O_3-TiO_2 NPs

The surface morphology of the acquired Fe_2O_3-Bi_2O_3-TiO_2 NPs was investigated using SEM and the obtained image is shown in Fi Figure 4 at 500 magnification level. FESEM image indicated that the Fe_2O_3-Bi_2O_3-TiO_2 NPs have smooth surfaces. In the SEM images, the agglomeration of NPs is also visible.

3.3 TEM Analysis of Fe_2O_3-Bi_2O_3-TiO_2 NPs

Figure 5 shows the TEM image at 500 magnification levels and corresponding size distribution histogram Fe_2O_3-Bi_2O_3-TiO_2 NPs. The figure indicates that Fe_2O_3-Bi_2O_3-TiO_2 NPs are uniform and cylindrical. A particle-size-distribution histogram determined from a TEM image showed a large variation in the particle sizes. The particles with an average diameter of 60 nm (Figure 6).

3.4 Magnetic properties

The magnetic properties of the synthesized nanocrystals were examined by using VSM at room temperature. The nanoparticles after heating at temperatures 200 to 500 °C are shown in Figure 7. The as-synthesized nanoparticles Ms value (Table 1) increases and then decreases on increasing calcination temperature from 200 to 500 °C. The increase of Ms may be an aspect of the
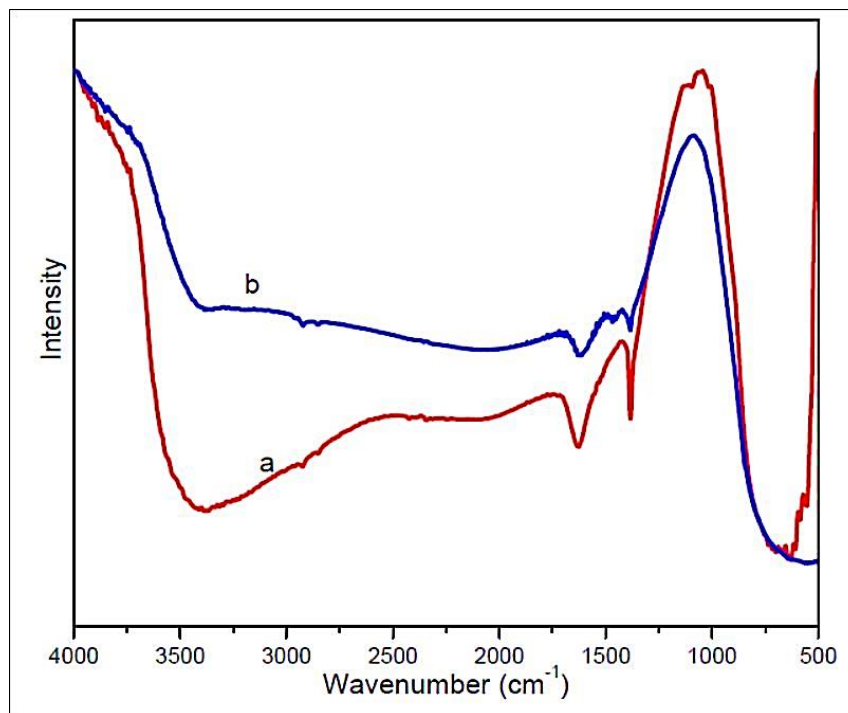
Fig 3. FTIR spectra of (a) Fe_2O_3-Bi_2O_3 (b) Fe_2O_3-Bi_2O_3-TiO_2
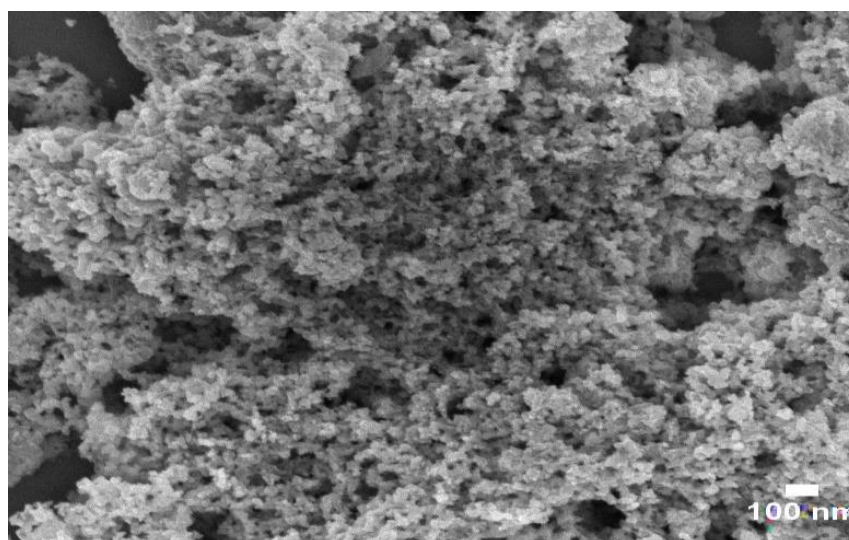
Fig 4. FESEM image of Fe_2O_3-Bi_2O_3-TiO_2 NPs
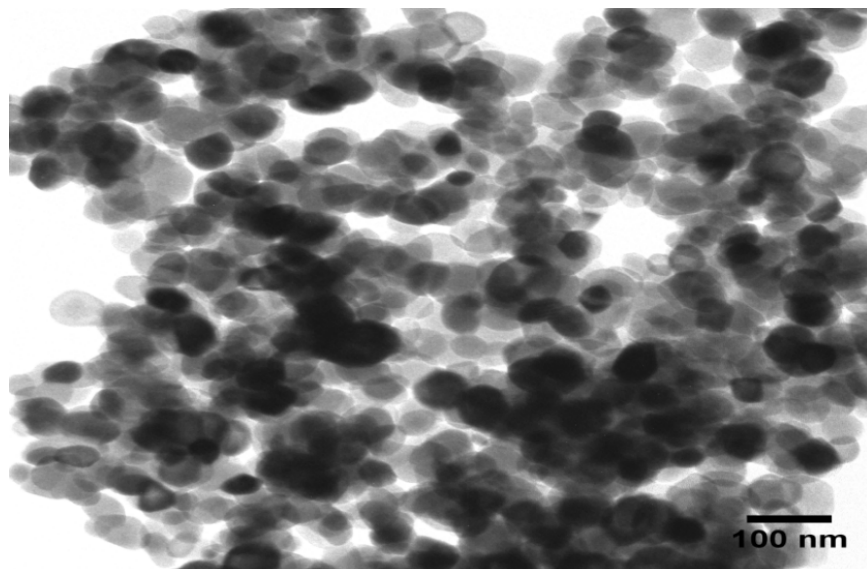
Fig 5. TEM image of Fe_2O_3-Bi_2O_3-TiO_2 NPs
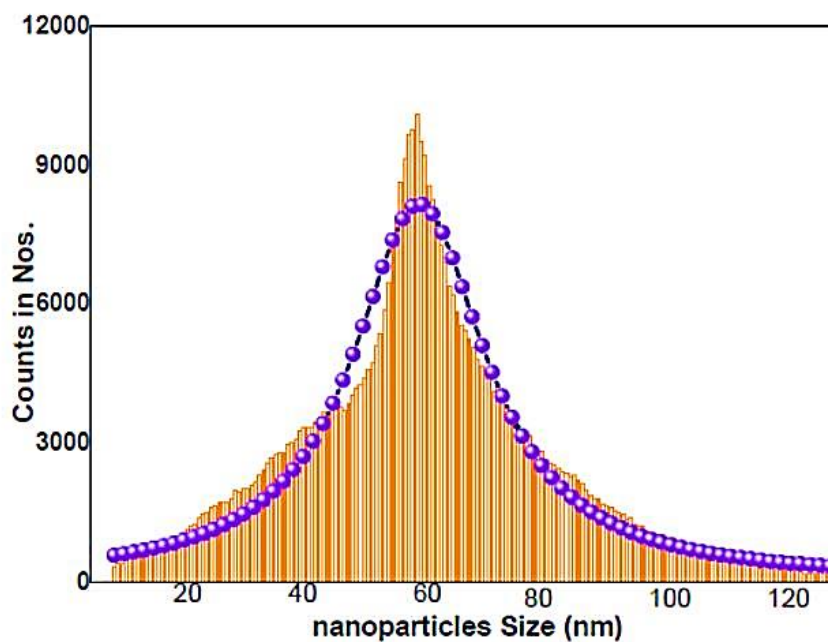
Fig 6. Particle size distribution curve of Fe_2O_3-Bi_2O_3-TiO_2 NPs

increase of particle size due to the coalescence of the particles by solid-state diffusion. By increasing calcination temperature from 400 to 500°C, Ms decreases respectively from 56 to 0.58 emu/g and the Hc increases respectively from 44.94 to 1190.3 Oe. This is due to the phase transition of ferromagnetic Fe_2O_3 to weak ferromagnetic α-Fe2O3 at 500°C. Otherwise, the coercivity value is low and in the single-domain ferromagnetic region, it sharply increases with increasing particle size.
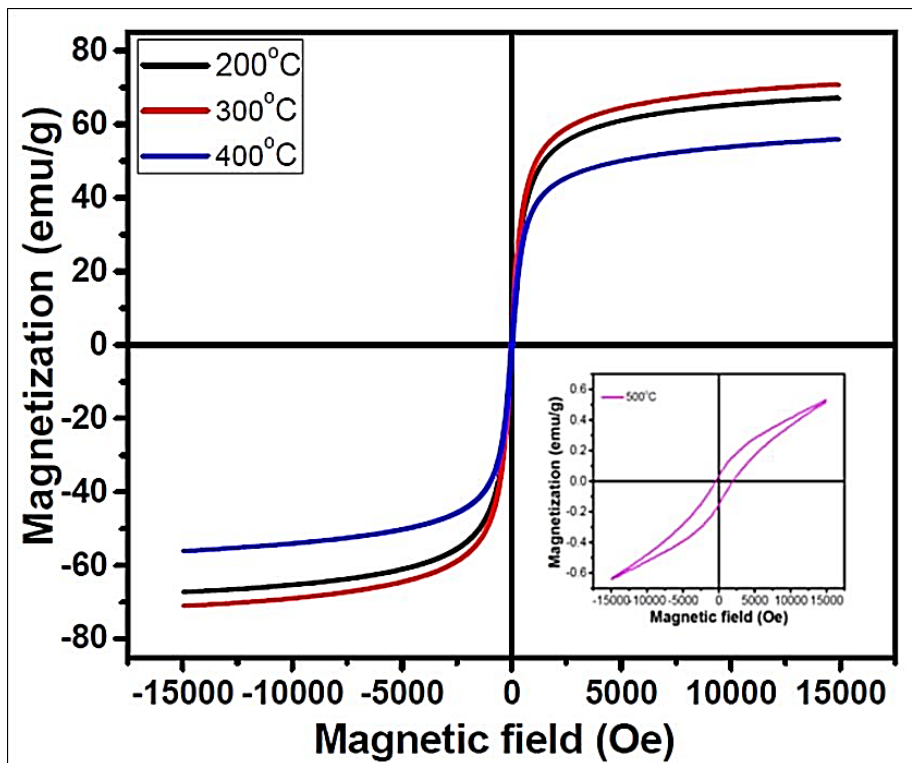
Fig 7. Magnetic hysteresis loops of the Fe_2O_3-Bi_2O_3-TiO_2 NPs obtained different calcination temperatures

Table 1. Change calcination temperature with the different magnetic property of Fe_2O_3-Bi_2O_3-TiO_2 NPs

T, ($^\circ$C)	M_s(emu/g)	H_c (Oe)	M_r , (emu/g)
200	63.02	29.03	2.91
300	69.11	32.02	3.48
400	56.41	45.12	3.87
500	0.59	1191.23	0.092

4 Conclusion

The Fe_2O_3-Bi_2O_3-TiO_2 NPs have been successfully prepared using the precipitation method. The prepared NPs were characterized by XRD, FT-IR, FE-SEM, UV-DRS spectra, and VSM, The XRD pattern of NPS shows the anatase phase, the obtained data from UV-Visible absorption spectra indicated that it was achieved through the process of Fe_2O_3 & Bi_2O_3 co-doping with TiO_2. Therefore, study suggests that the introduction of Fe_2O_3 & Bi_2O_3 can effectively control the selective crystallization of the anatase phase of TiO_2. The effect of calcination on the magnetic and structural properties of Fe_2O_3-Bi_2O_3-TiO_2 NPs was studied. The Fe_2O_3-Bi_2O_3-TiO_2 NPs by calcination up to 300 $^\circ$C, magnetite converted to maghemite, the second transition is in the range 400 – 500 $^\circ$C to change hard ferromagnetic hematite.

References

1) Huang CC, Hung YH, Kuo MF. Investigation of the influence of raw material Fe2O3 on the magnetic properties of Sr-ferrite magnets. Funai Oyobi Fummatsu Yakin. *Journal of Japan Society of Powder and Powder Metallurgy*. 2016;63(7):636–642. doi:10.2497/jjspm.63.636.
2) Kawano S, Kosuge K, Kachi S. Electric and Magnetic Properties of "VO". *Journal of the Physical Society of Japan*. 1966;21(12):2744–2745. doi:10.1143/jpsj.21.2744.
3) Noval VE, Universitaria C. Fe3O4 -TiO2 and Fe3O4 -SiO2 Core-shell Powders Synthesized from Industrially Processed Magnetite (Fe3O4) Microparticles. *Materials Research*. 2019;22(3):1–12.

4) Chirita M, Grozescu I. Fe2O3 - Nanoparticles , Physical Properties and Their Photochemical And Photoelectrochemical Applications. *Chem Bull Politeh Univ Timsisoara*. 2009;54(68):1–8.

5) Rymarczyk J, Hanc A, Dercz G, Ilczuk J. Mössbauer Spectroscopy X-Ray Diffraction and SEM Studies on Multiferroic Bi5Ti3FeO15Ceramics. *Acta Physica Polonica A*. 2008;114:1579–1584. doi:10.12693/aphyspola.114.1579.

6) Balamurugan S, Balu AR, Narasimman V, Selvan G, Usharani K, Srivind J, et al. Multi metal oxide CdO–Al2O3–NiO nanocomposite—synthesis, photocatalytic and magnetic properties. *Materials Research Express*. 2018;6(1):015022–015022. doi:10.1088/2053-1591/aae5af.

7) Gich M, Frontera C, Roig A, Taboada E, Molins E, Rechenberg HR, et al. High- and Low-Temperature Crystal and Magnetic Structures of ε-Fe2O3and Their Correlation to Its Magnetic Properties. *Chemistry of Materials*. 2006;18(16):3889–3897. doi:10.1021/cm060993l.

8) Laurent S, Boutry S, Muller RN. Metal Oxide Particles and Their Prospects for Applications. Elsevier Ltd. 2018;p. 3–42. doi:10.1016/B978-0-08-101925-2.00001-2.

9) Lomanova NA, Gusarov VV. Electrical properties of perovskite-like compounds in the Bi2O3-Fe2O3-TiO2 system. *Inorganic Materials*. 2011;47(4):420–425. doi:10.1134/s0020168511040169.

10) Guo X, Liu J, Guo G. Photocatalytic Removal of Dye and Reaction Mechanism Analysis over Y2O3 Composite Nanomaterials. In: and others, editor. MATEC Web Conference;vol. 88. 2016;p. 1–5. Available from: 10.1051/matecconf/20178802003.

11) Praveena K, Sadhana K, Srinath S, Murthy SR. Effect of TiO2 on electrical and magnetic properties of Ni0.35Cu0.12Zn0.35Fe2O4 synthesized by the microwave–hydrothermal method. *Journal of Physics and Chemistry of Solids*. 2013;74(9):1329–1335. doi:10.1016/j.jpcs.2013.04.014.

12) Singh SP, Karmakar B. Bismuth oxide and bismuth oxide doped glasses for optical and photonic applications. . In: and others, editor. In: Bismuth: Characteristics, Production and Applications. Materials Science and Technologies. 2012;p. 229–249. Available from: http://cgcri.csircentral.net/id/eprint/1384.

13) Jartych E, Pikula T, Mazurek M, Franus W, Lisinska-Czekaj A, Czekaj D, et al. Structure and Magnetic Properties of Bi5Ti3FeO15 Ceramics Prepared by Sintering, Mechanical Activation and Edamm Process. A Comparative Study. *Archives of Metallurgy and Materials*. 2016;61(2):869–874. doi:10.1515/amm-2016-0147.

14) Wang F, Yu L. Corn-like, recoverable γ-Fe 2 O3-SiO2 @TiO2 photocatalyst induced by magnetic dipole interactions. *Scientific Reports*. 2017;7(1):2–11. doi:10.1038/s41598-017-07417.

15) Kaur N, Shahi SK, Singh V. Synthesis, characterization and photocatalytic activity of magnetically separable γ-Fe2O3/N,Fe codoped TiO2 heterojunction for degradation of Reactive Blue 4 dye. *RSC Advances*. 2015;5(76):61623–61630. doi:10.1039/c5ra07812a.

16) Gasmalla HB, Lu X, Shinger MI, Ni L, Chishti AN, Diao G. Novel magnetically separable of Fe3O4/Ag3PO4@WO3 nanocomposites for enhanced photocatalytic and antibacterial activity against Staphylococcus aureus (S. aureus). *Journal of Nanobiotechnology*. 2019;17(1). doi:10.1186/s12951-019-0485-z.